N92-14353

MEASUREMENTS OF PRESSURE DISTRIBUTIONS AND FORCE COEFFICIENTS IN A SQUEEZE FILM DAMPER - PART II: PARTIALLY SEALED CONFIGURATION

S.Y. Jung, L.A. San Andres, and J.M. Vance
Department of Mechanical Engineering
Texas A&M University
College Station, Texas 77843-3123, U.S.A.

In part I, a squeeze film damper (SFD) test rig and measurement procedures were explained, and the experimental results obtained from an open ended damper were presented. In this paper, the experimental results measured from a partially sealed SFD test rig executing a circular centered orbit are presented and discussed. A serrated piston ring is installed at the damper exit. This device involves a new sealing concept which produces high damping values while allowing for oil flow to cool the damper. In the partially sealed damper, large cavitation regions are observed in the pressure fields at orbit radii $\epsilon = 0.5$ and $\epsilon = 0.8$. The cavitated pressure distributions and the corresponding force coefficients are compared with a cavitated bearing solution. The experimental results show the significance of fluid inertia and vapor cavitation in the operation of squeeze film dampers. Squeeze film Reynolds numbers tested reach up to Re=50, spanning the range of contemporary applications.

NOMENCLATURE

C	=SFD radial clearance
C_{dRe}	$=\rho\omega LR^3/C$ damping coefficient conversion factor
C_{iRe}	$=\rho LR^3/C$ inertia coefficient conversion factor
C_f	$=\mu\omega R^3 L/C^2$ force conversion factor
C_p	$=\mu\omega R^2/C^2$ pressure conversion factor
C_{pRe}	$=C_p \cdot Re = \rho\omega^2 R^2$ pressure conversion coefficient
C_{tt}	=dimensionless direct damping coefficients
	$=-f_t/\epsilon$, normalized by $\mu R^3 L/C^3$
D	=damper journal diameter
D_{rr}	=dimensionless direct inertia coefficients
	$=f_r/\epsilon$, normalized by $\mu R^3 L/\omega C^3$
f_r f_t	=dimensionless radial and tang. film forces normalized by C_f
	$=\int p\cos\theta d\theta$, $\int p\sin\theta d\theta$, respectively.

L	=damper journal length
p	=dimensionless pressure normalized by C_p
R	=damper journal radius
Re	$=\omega C^2/\nu$ modified Reynolds number
Z	=axial coordinate
ϵ	=dimensionless orbit radius
θ	=circumferential coordinate
θ_a	=cavitation termination position
θ_c	=cavitation inception position
μ	=absolute viscosity
ν	=kinematic viscosity
ρ	=density
ϕ	$=90^\circ + \tan^{-1} f_r/f_t$, phase angle
ω	=frequency of damper journal center motion

INTRODUCTION

In Part I, a companion paper, a squeeze film damper (SFD) test apparatus and experimental procedure were detailed, and the experimental results obtained for an open ended configuration were presented and compared with a modified short bearing solution.

In this paper, the experimental results measured from a partially sealed SFD test rig executing a circular centered orbit are presented. The squeeze film damper is sealed with a serrated piston ring to partially prevent side leakage of lubricant so that the damping capability of the damper is increased. The serrated piston ring is described in detail and its function is explained in the next section. The experimental conditions are the same as in the open ended SFD test rig described in Part I.

In the partially sealed damper, a large cavitation region in the pressure field is observed at orbit radii $\epsilon = 0.5$ and $\epsilon = 0.8$. The cavitated pressure distributions and the corresponding force coefficients (both damping and inertia) are compared with a cavitated bearing solution. The squeeze film Reynolds number tested are within the range of contemporary applications.

EXPERIMENTAL TEST RIG AND PROCEDURE

The overall structure of the damper test rig and experimental procedure have been described in detail in Part I and thus, related details are omitted here. Figure 1 shows the axial geometry of the partially sealed SFD configuration. A serrated piston ring (see Figure 2) is placed at the cavity (or piston ring groove) at the end of damper journal. The other experimental conditions, such as oil supply pressure and locations of pressure and temperature transducers, are the same as described in Part I. However, in the partially sealed damper, the

oil temperature increases more rapidly because of the reduced axial flow rates through the damper.

With a uniform conventional piston ring located at the damper end, early experimental measurements showed that no leakage through the end seal occured. Under this condition, measured film pressures and forces reproduced closely the predictions given for the fully sealed SFD model. Therefore, the levels of damping forces obtained were large and quite accurately predicted with the inertial SFD fluid flow model [1].

Since a damper without through flow does not represent conditions found in practice, the piston ring end seal was modified to allow some amount of oil leakage. The idea of enlarging the circumferential groove in which the piston ring is located was discarded after experiments indicated that the piston ring cocks in the groove and distorts the pressure field. A piston ring with a radial split was also found not attractive since the pressures would be distorted due to the localized jet effect at the piston ring opening.

A piston ring with a large number of small axial grooves around the circumference allows a sufficient amount of oil circulation, and does not distort the rotating pressure field. This condition is only insured provided that the lubricant inlet pressures are not too large so as not to induce distorting effects at the inlet holes in the squeeze film.

As shown by a schematic drawing in Figure 2, the serrated piston ring consists of a piston ring of inner and outer diameters equal to 12.23 cm (4.816 inch) and 13.02 cm (5.125 inch), respectively, and with thickness and width equal to 3.97 mm (5/32 inch). 72 semi-circular holes of radius 0.79 mm (1/32 inch) are drilled every 5° on the outer surface of the piston ring. The total area of grooves is 8 times larger than the area of the inlet holes. This number was chosen so that the total pressure loss factor for the holes in the piston ring is similar to the loss factor at the inlet holes.

Preminary experiments were aimed to determine, first, if the rotating pressure wave was distorted by the presence of the piston ring holes, and second, to measure the absolute levels of film pressure generated in the squeeze film region.

The preminary tests showed that the film pressure wave was not distorted and remained stationary with respect to the rotating shaft. Therefore, a single pressure transducer was needed to reproduce the pressure field around the journal surface.

The most important preliminary finding was that film cavitation did occur as the observed dynamic pressure waves showed a uniform region of minimum dynamic pressures. Experimental measurements of absolute pressure showed that the region of film cavitation represented pressures which are close to zero absolute. Thus, it is presumed that the form of cavitation observed in the experimentation corresponded to incipient boiling (vapor cavitation) of the lubricant at low values of absolute pressure.

From the discussion above, it is apparent that the measurements show the film pressure to attain large levels of subatmospheric pressures, which remain during a substantial portion of the total time required to describe a complete journal orbit. This comment is made here since current theoretical treatments often consider film cavitation to start at pressure levels very close, but lower than, atmospheric pressure. This form of cavitation relates to the release of air dissolved in the oil or the ingress of external air in the film region, and is likely to occur if the damper is not completely flooded in oil [2].

The partially sealed damper, due to the reduced side leakage, produces a smaller axial pressure drop and larger peak pressures and damping levels when compared to the open end damper. The most important outcome of this is that the pressure field is significantly disturbed due to the large extent of vapor cavitation in the pressure field. In this case, the supply pressure can not be large enough to suppress the cavitation. Because higher supply pressures to suppress the cavitation produce enough flow through the check valves to hold them open and produce distortion of the pressure wave due to backflow through the inlet holes. Consequently the damping level achieved from the partially sealed damper can be greatly reduced or widely varied depending on the extent of vapor cavitation taking place in the pressure profiles. Another important factor is fluid inertia which tends to move the position of cavitation inception toward the minimum film gap and to decrease the peak pressure [3,4].

The following experimental measurements show the effects of vapor cavitation and fluid inertia on the pressure fields and force coefficients.

EXPERIMENTAL RESULTS AND DISCUSSIONS

Pressure profiles

Figures 3 and 4 show the dimensionless dynamic film pressure distribution vs. time at axial locations, Z1 and Z2, for orbit radii $\epsilon = 0.47$ and 0.76, respectively. Reynolds numbers are Re=2.07 and 2.3, respectively. These pressure profiles are significantly affected by vapor cavitation. As described before, the cavitation pressure is close to zero absolute. The damper is completely submerged in oil which prevents the ingress of external air. Thus, it is presumed that the measured cavitation here corresponds to vapor cavitation.

In these figures, the double dotted lines are the pressure profiles predicted at the two axial locations Z1 and Z2 by the cavitation analysis [3,4]. The analysis includes extended cavitation effects on the pressure distribution using the Swift-Stieber conditions [5,6]. In order to compare experimental measurements with the cavitated pressure predictions, the predicted absolute pressure profile has been shifted to the measured dynamic pressure profile, because the measurement with the absolute pressure transducer established the cavitation pressure here as absolute zero. To predict the cavitated pressure field, the position θ_a of cavitation termination is taken from the measured pressure profile and leakage

coefficient values, $CL_l = 0.0$ and $CL_r = 0.18$, are used. The cavitation end points for $\epsilon = 0.47$ and $\epsilon = 0.76$ are about $\theta_a = 30°$ and $\theta_a = 350°$, respectively, as shown in Figures 3 and 4. $\theta_c = 141.3°$ and $\theta_c = 158.7°$ are predicted by the analysis as the corresponding positions of cavitation inception, respectively. The prediction of cavitation inception points and the whole of the pressure field agrees well with the experimental measurement. The above comparisons using the Swift-Stieber conditions show that the cavitation effect is significant on pressure distributions.

Generally, a much larger level of the measured peak pressure is expected from the partially sealed damper when compared to that from the open ended damper (see Part I). But at small Reynolds numbers the peak pressure measured from the partially sealed damper is only slightly larger than that obtained from the open ended damper. The two main reasons for this are 1) a smaller orbit radius of the partially sealed damper and 2) a larger extent of vapor cavitation in the pressure fields. The peak pressure of a SFD or a journal bearing is so sensitive to large orbit radius or eccentricity ratio that a small reduction of orbit radius causes a large reduction of the peak pressure. Furthermore, as shown in the vapor cavitation analysis [3], the peak pressure is greatly reduced as the extent of the vapor cavitation increases.

Figure 5 depicts pressure waves measured at Reynolds number equal to Re=22.1 and an orbit radius $\epsilon = 0.81$. As shown in the previous pressure comparison, the double dotted line is the pressure profile predicted at the axial location Z1 using the cavitation analysis which includes vapor cavitation effects on the pressure field. The position θ_a of cavitation termination is $\theta_a = 130°$ which was taken from the measured pressure profile. But, instead of the seal coefficients $CL_l = 0.0$ and $CL_r = 0.18$, the seal coefficients $CL_l = CL_r = 0.0$ are required, which implies no side leakage from the damper.

The prediction of pressure profiles using the analysis gets degraded as the Reynolds number becomes large, because an assumption that fluid inertia does not affect the velocity profiles is used in the cavitated long bearing analysis [3]. The assumption is valid for Re$\leq$10. Thus, as shown in Figure 5, the prediction is not good at large Reynolds number (note the different seal coefficients required), and also the pressure profiles shown in Figure 6 which were measured using DOW10 oil, can not be compared with any predictions. However, it is very interesting to compare these pressure profiles with those of the open ended damper.

The relevant difference between these configurations are

1) The peak pressures measured from the partially sealed damper are much larger than those from the open ended damper.

2) As orbit radius increases, the extent of cavitation greatly increases. The pressure profiles of the partially sealed damper are more extensively cavitated than those of the open ended damper.

3) The pressure profiles of the partially sealed damper show less fluid inertia

effects than those of the open ended damper. The main effects of fluid inertia on the pressure profile are that the positive peak pressure is smaller than the negative peak pressure, and the pressure has a negative value at the minimum film thickness region ($\omega t = 0$) while it has a positive value at the maximum film thickness region ($\omega t = \pi$). Moreover, as fluid inertia becomes dominant in the film forces, the shape of the pressure profile tends to change from antisymmetric to symmetric with respect to the maximum film thickness. The measured pressure profiles of the partially sealed damper are fairly antisymmetric, while the pressure profiles of the open ended damper are more symmetric with respect to $\omega t = \pi$ at large Reynolds numbers.

Force coefficients

Local damping and inertia coefficients and phase angles for orbit radii equal to $\epsilon = 0.5$ and 0.8 are obtained by integrating the measured pressure field around the journal of the damper. Since the measured pressure wave has been determined to be synchronous with speed, the relation of the pressure/time curve to that of pressure/angle curve around the journal surface is well known. In the numerical calculations, the entire pressure wave has been used to determine film forces and force coefficients. The pressure signals at orbit radius $\epsilon = 0.5$ with large Reynolds numbers were not large enough to measure so that the corresponding force coefficients are presented here.

Figures 7 show the local damping coefficients C_{tt} measured at the axial locations Z1 and Z2. Since the measured pressure fields at small Reynolds number are greatly cavitated, as shown in the previous pressure profiles, these damping coefficients shown in Figure 7(a) represent the equivalent damping coefficients C_{eq} equal to $(C_{tt} - D_{tr})$.

In Figure 7(a), the solid lines are predictions of damping coefficients at the axial location Z1 for $\epsilon = 0.5$ and 0.8. These lines are obtained from a curvefit of damping coefficients predicted from a cavitated bearing solution [3,4], based on the measured cavitated pressure profiles. Considering the effect of vapor cavitation on the entire pressure field, the predictions of damping coefficients are fairly matched with the measurements. Figure 7(b) shows comparison of damping coefficients at large Reynolds numbers where cavitation disappeared. Thus an uncavitated model is used to calculate the damping coefficients with the seal coefficients $CL_l = CL_r = 0.0$. The predicted damping coefficients remain constant for increasing Reynolds numbers.

The level of local damping achieved from the partially sealed damper is about twice that from the open ended damper for the whole range of Reynolds numbers. The actual (dimensional) damping can be determined if the measured dimensionless damping coefficients C_{tt} are multiplied by the damping conversion factor C_{dRe}/Re. (see Table I of Part I)

Figures 8 show the local inertia coefficients D_{rr} at the axial locations Z1 and Z2. For Reynolds numbers below Re=10 in Figure 8(a), the local inertia force

coefficients D_{rr} represent the equivalent inertia coefficients $D_{eq} = D_{rr} - C_{rt}$ due to the cavitation taking place in the pressure field (Figures 3 to 5). Once again the solid lines in Figure 8(a) are predictions of inertia coefficients obtained from the cavitated bearing solution [3,4]. The predictions are fairly matched with the measurements. However, the solid line in Figure 8(b) represents a prediction of inertia coefficients calculated from an uncavitated film model with the seal coefficients $CL_l = CL_r = 0.0$.

When compared with the inertia coefficients measured from the open ended damper, the (negative) values of the equivalent inertia coefficients from the partially sealed damper are about twice as much as at small Reynolds number, due mainly to the large cross coupled damping coefficient ("dynamic stiffness") caused by the cavitated pressure field. However, for large Reynolds number, the pure inertia coefficients of the partially sealed damper show the same magnitude as those of the open ended damper, while the pure damping coefficients of the partially sealed damper are about three times as those of the open ended damper. Therefore, the ratio of the fluid inertia force to the fluid viscous force measured from the partially sealed damper is less than that of the open ended damper. That is, the partially sealed damper has been less influenced by fluid inertia than the damper with open ends. This phenomenon was also found in the comparison of pressure distributions measured from the two types of squeeze film dampers.

The force phase angle ϕ determined from the ratio of the radial film force to the tangential film force is shown in Figures 9. The predictions are good as shown in Figure 9(a). Since the pressure profiles at Reynolds numbers less than Re=10 are greatly cavitated, phase angles are below $\phi = 90°$. But as Reynolds number increases, the extent of cavitation is reduced and the fluid inertia force is dominant so that phase angle becomes larger than $\phi = 90°$ as shown in Figure 9(b).

CONCLUSIONS

Experimental tests have been performed on a partially sealed squeeze film dampers to measure fluid film pressure distributions and force coefficients with circular centered orbits with both $\epsilon = 0.5$ and 0.8. The measurements performed completely cover the practical range of Reynolds number which reaches Re=50.

From the experimental measurements described, the following conclusions can be obtained

1) There is a small pressure drop in the axial direction. It is thus apparent that the partially sealed configuration will give substantial levels of damping due to the uniformity of the pressure in the axial direction.

2) However, the present experimental results show that the development of the region of negative dynamic pressure is sharply detained by vapor cavitation. The extent of vapor cavitation greatly reduces both damping and inertia coefficients, and the phase angles are below 90°.

3) The extent of cavitation is larger at low Reynolds numbers (lowest temperature) than at higher Reynolds numbers. This is due to the effect of increasing temperature which diminishes the fluid viscosity and consequently, reduces the level of generated pressures.

4) The partially sealed configuration has been less influenced by fluid inertia than the open ended configuraton. Larger extent of vapor cavitation region has been observed in the partially sealed configuration than in the open ended configuration. The effect of cavitation must be properly included in the analysis if accurate predictions are to be made.

ACKNOWLEDGMENTS

The support by the Turbomachinery Research Consortium at Texas A&M University is greatly acknowledged.

REFERENCES

[1] San Andres, L. A., "Effect of Fluid Inertia on Squeeze Film Damper Force Response", Ph.D. Dissertation, Dept. of Mechanical Eng., Texas A&M University, December 1985

[2] Zeidan, F. Y., "Cavitation Effects on the Performance of Squeeze Film Damper Bearings", Ph.D. Dissertation, Dept. of Mechanical Eng., Texas A&M University, August 1989

[3] Jung, S. Y. and Vance, J. M., "Effects of Vapor Cavitation and Fluid Inertia on the Force Coefficients of a Squeeze Film Damper, Part I- Analysis of a Long Squeeze Film Damper", to be presented at the 1990 annual meeting of STLE in Denver

[4] Jung, S. Y. and Vance, J. M., "Effects of Vapor Cavitation and Fluid Inertia on the Force Coefficients of a Squeeze Film Damper, Part II- Experimental Comparisons", to be presented at the 1990 annual meeting of STLE in Denver

[5] Swift, H. W., "The Stability of Lubricating Films in Journal Bearings", *Proceedings Institute of Civil Engineers*, Vol. 233, London, 1932, pp. 267-288

[6] Stieber, W., "Das Schwimmlager", VDI, Berlin, 1933

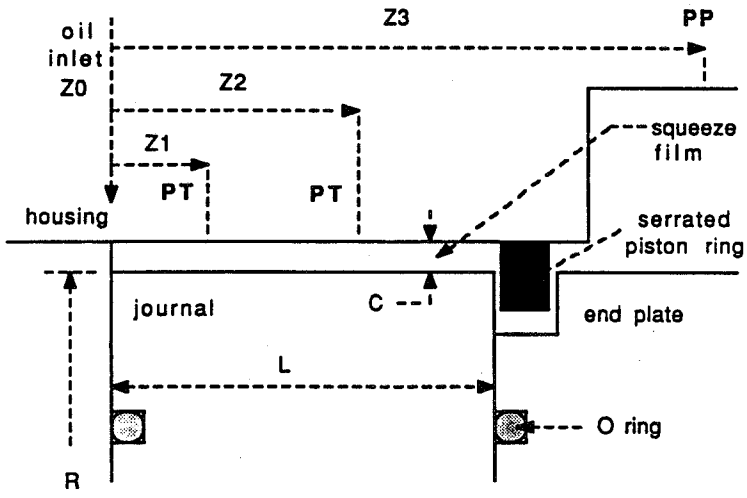

L/D=0.188

Z1=0.56 cm (0.2200 inch)
Z2=1.67 cm (0.6575 inch)
Z3=3.71 cm (1.4600 inch)

L=2.39 cm (0.94 inch)
R=6.35 cm (2.50 inch)
C=0.159 cm (0.0625 inch)

PT : Pressure Transducer

PP : Proximity Probe

Fig. 1 SFD geometry of a partially sealed configuration

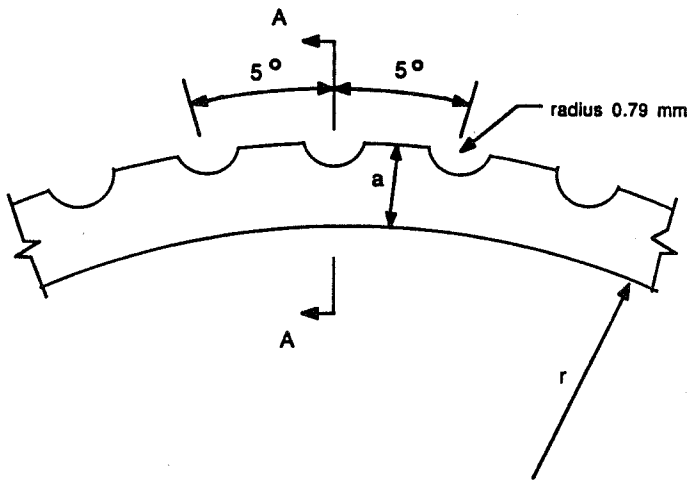

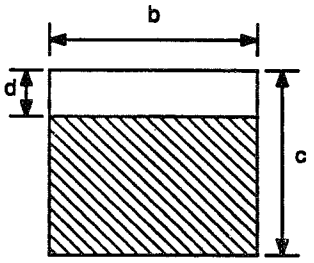

Section A-A

a=3.97 mm (5/32 in)
b=3.97 mm (5/32 in)
c=3.97 mm (5/32 in)
d=0.79 mm (1/32 in)
r=61.2 mm (2.408 in)

(Note : 72 holes of radius 0.79 mm are equally spaced)

Fig. 2 Geometry of a serrated piston ring

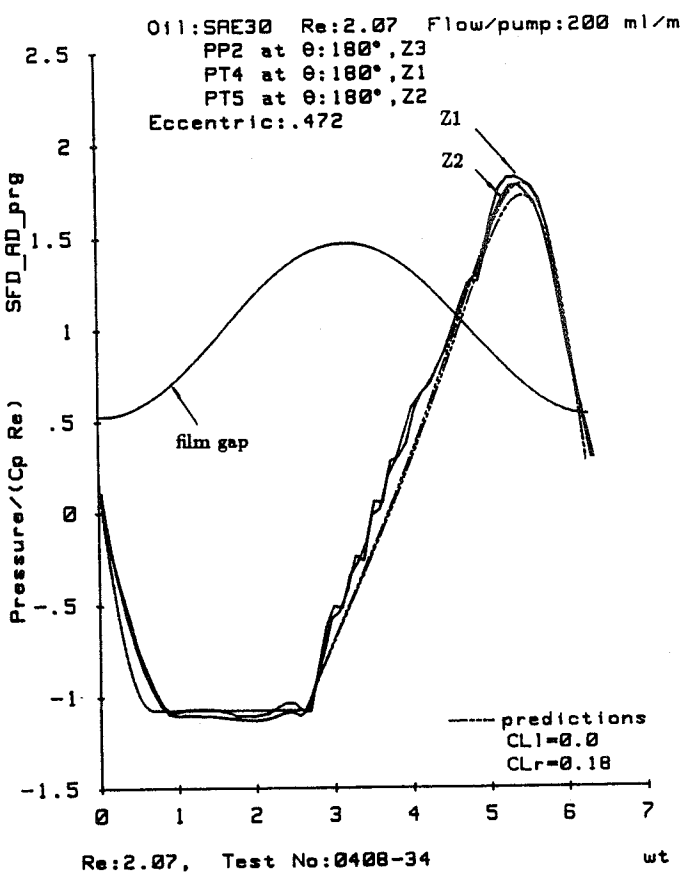

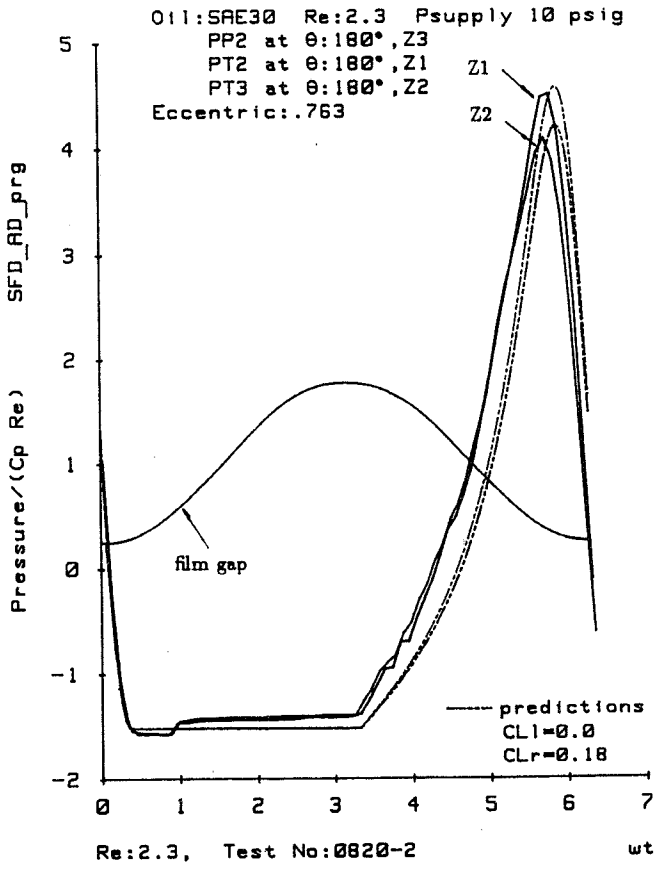

Fig. 3 Dimensionless pressure profiles, partially sealed configuration, Re=2.07, $\epsilon = 0.47$

Fig. 4 Dimensionless pressure profiles, partially sealed configuration, Re=2.3, $\epsilon = 0.76$

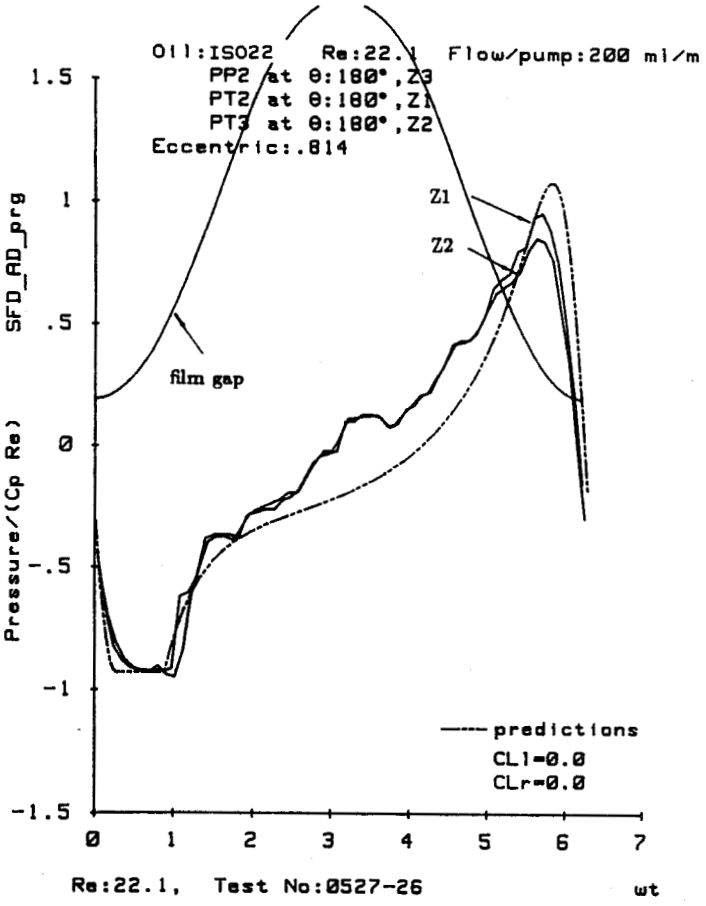

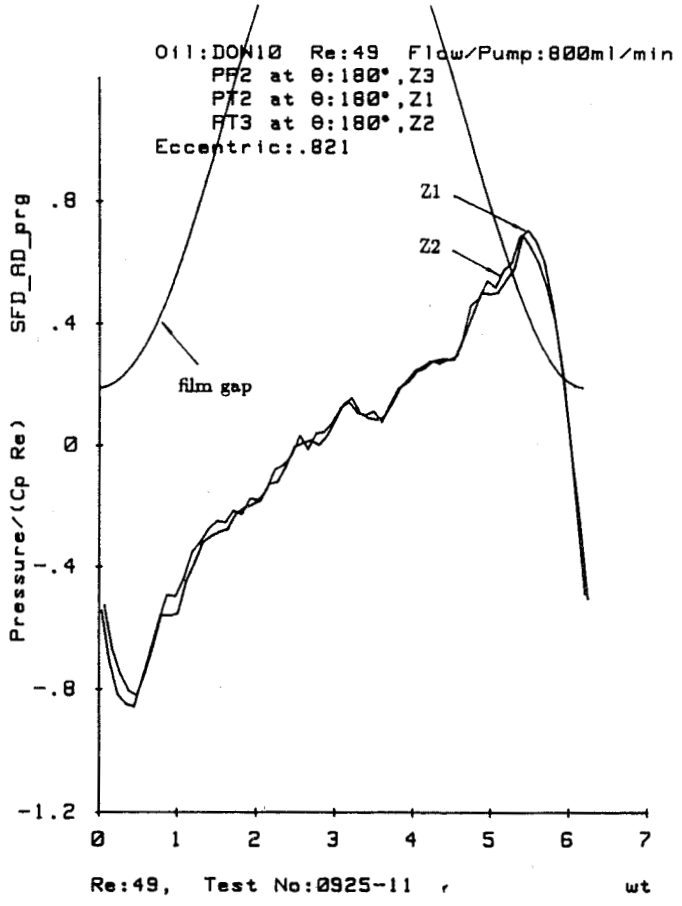

Fig. 5 Dimensionless pressure profiles, partially sealed configuration, Re=22.1, $\epsilon = 0.81$

Fig. 6 Dimensionless pressure profiles, partially sealed configuration, Re=49.0, $\epsilon = 0.82$

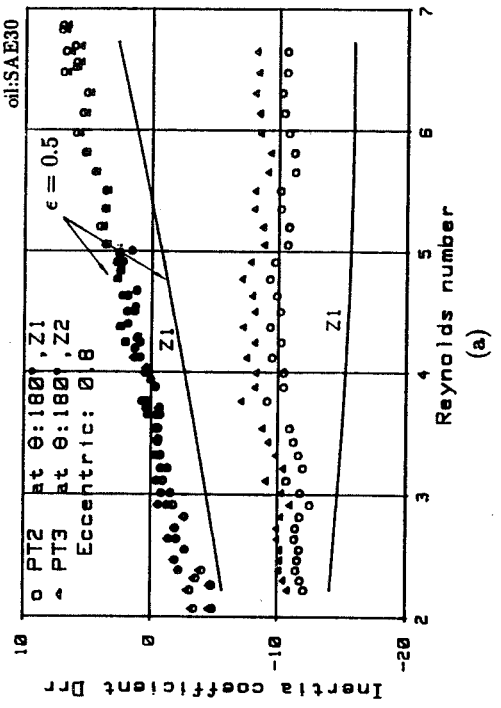

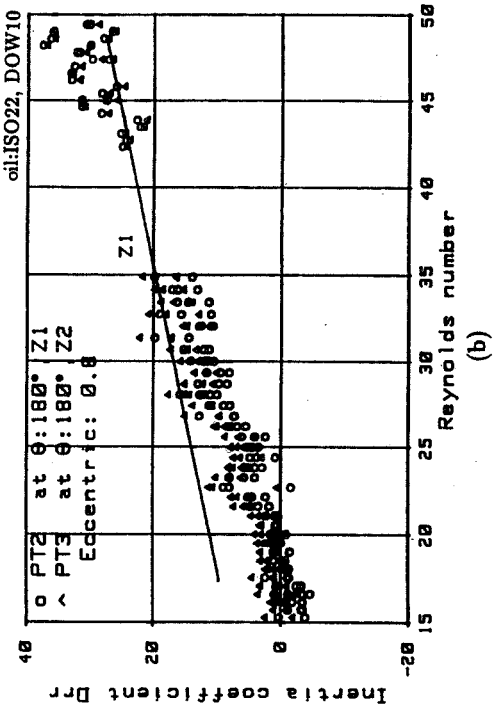

Fig. 8 Dimensionless inertia coefficients vs. Reynolds no.

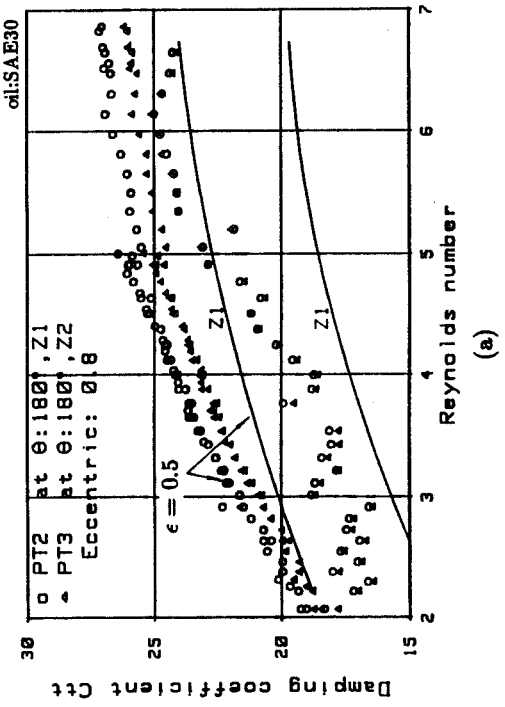

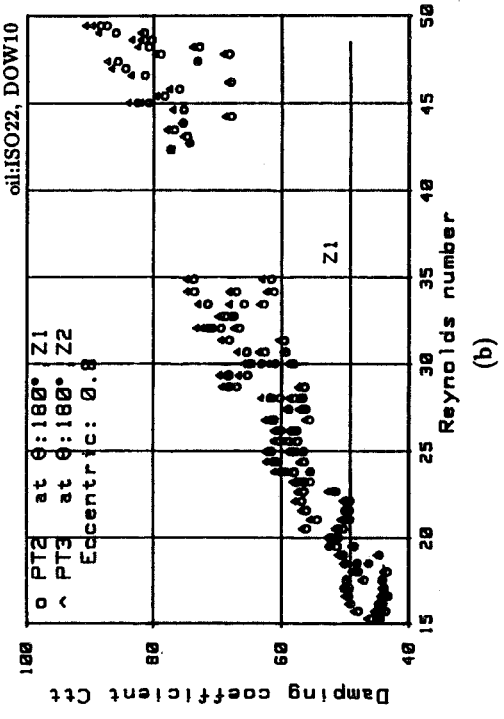

Fig. 7 Dimensionless damping coefficients vs. Reynolds no.

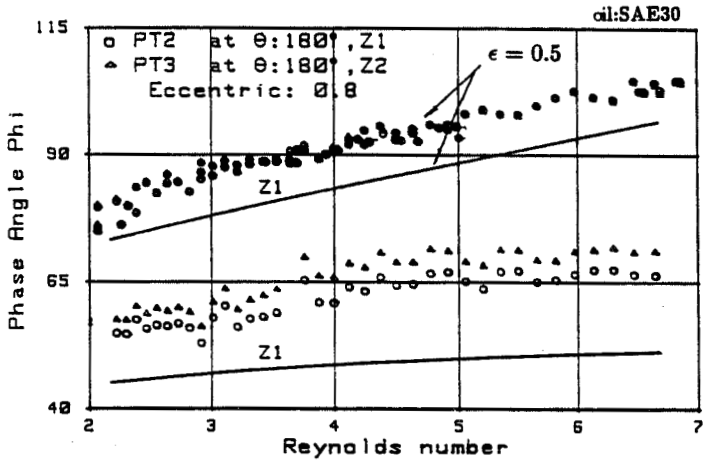

(a)

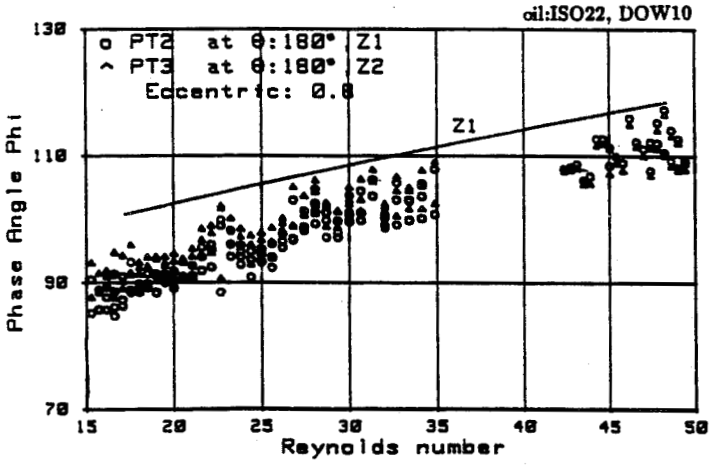

(b)

Fig. 9 Phase angle vs. Reynolds number